

Residual static strength of cracked concrete-filled circular steel tubular (CFCST) T-joint

M.J. Cui and Y.B. Shao *

*School of Civil Engineering, Yantai University,
Qingquan Road 32#, Laishan District, Yantai, Shandong Province, PR China, 264005*

(Received May 07, 2013, Revised October 22, 2014, Accepted October 29, 2014)

Abstract. Concrete-filled circular steel tubular joints (CFSTJs) in practice are frequently subjected to fluctuated loadings caused by wind, earthquake and so on. As fatigue crack is sensitive to such cyclic loadings, assessment on performance of CFSTJs with crack-like defect attracts more concerns because both high stress concentration at the brace/chord intersection and welding residual stresses along weld toe cause the materials in the region around the intersection to be more brittle. Once crack initiates and propagates along the weld toe, tri-axial stresses in high gradient around the crack front exist, which may bring brittle fracture failure. Additionally, the stiffness and the load carrying capacity of the CFSTJs with crack may decrease due to the weakened connection at the intersection. To study the behaviour of CFSTJs with initial crack, experimental tests have been carried out on three full-scale CFCST T-joints with same configuration. The three specimens include one uncracked joint and two corresponding cracked joints. Load-displacement and load-deformation curves, failure mode and crack propagation are obtained from the experiment measurement. According to the experimental results, it can be found that the load carrying capacity of the cracked joints is decreased by more than 10% compared with the uncracked joint. The effect of crack depth on the load carrying capacity of CFCST T-joints seems to be slight. The failure mode of the cracked CFCST T-joints represents as plastic yielding rather than brittle fracture through experimental observation.

Keywords: concrete-filled circular steel tubular T-joint (CFCST T-joint); experimental study; fatigue crack; residual static strength; failure mode

1. Introduction

Due to the advantages of beautiful configuration, simple style, high strength-weight ratio etc., tubular structures are extensively applied in many fields such as long-span bridge, stadium, high-rise tower and so on. However, much attention should be paid to the problems which are caused by several external environment factors, including wind, sea wave, earthquake and so forth.

As those structures are consisted of tubular joints, formed by welding several smaller tubes (so-called brace) together onto a large tube member (namely chord), residual stress can be generated at the brace/chord intersection, where fatigue crack can occur easily under cyclic loadings. The fatigue crack propagates continuously under cyclic loading, and the net cross section

*Corresponding author, Ph.D., Professor, E-mail: cybshao@ytu.edu.cn

area of the intersection decreases gradually with crack propagation. The development of the fatigue crack also causes much more severe stress concentration around crack front. When the crack size becomes very large, the welded tubular structures may fail as sudden fracture due to severe deterioration of the static strength at the joint position.

To study the fracture behaviour of tubular structures, one of universal and practical methods is fracture mechanics approach. This method is based on the information about the material properties (such as toughness of steel material), the size of crack, and the fatigue life of structures. Therefore, the fracture behaviour of tubular structures can be measured by failure assessment diagram, which represents the relationship between stress intensity factor (K_I) and the applied load (P). In the literature, some studies based on this method have been reported by carrying out experimental tests to assess the integrity of tubular joints. Among these research works, Zerbst (Zerbst and Miyata 2002, Zerbst *et al.* 2002a, b) studied the fracture behaviour of welded tubular T-joint with hollow section and evaluated the accuracy and validity of different types of failure assessment methods with the experimental results. However, this study cannot represent the behaviour of the joints in practical engineering, where the location and size of crack is undetermined, because the crack is artificial and not fabricated by fatigue test.

Due to the complexity of fatigue crack, the numerical model of the cracked joints cannot be obtained easily from some commercial finite element software such as ABAQUS. Hence, many studies have been carried out to generate the finite element model of tubular joints with crack. For cracked tubular joints with hollow section, the study of residual static strength has been carried out. Lie *et al.* (2004, 2006a, b, 2007, 2009) studied the fracture behaviour of tubular joints with fabricated crack from static strength, where the residual static strength of hollow section tubular T-joints is estimated by using experimental and numerical methods (Lie *et al.* 2006a, b). Meanwhile, through analyzing the experimental results, the accuracy of failure assessment diagram is obtained. In addition, the residual static strengths of high strength steel cracked tubular T- and Y-joints with hollow section have been conducted by Talei-Faz *et al.* (2004). The results show that the load carrying capacity of the high strength steel tubular joints is not greatly affected by relative large cracked sections. Similarly, Song and Shao (2012) carried out experimental research on the influence of surface fatigue cracks on the static strength of circular tubular T-joints. It can be found that the static strength of the cracked tubular T-joints under axial tensile loading is decreased compared with that of T-joint without any defects.

However, all the above researches are only focused on cracked tubular joints with hollow section, and the studies on the residual static strength of cracked concrete-filled circular steel tubular (CFCST) joints are rarely reported. Therefore, it is a valuable work to conduct some investigations on the residual strength of CFCST joints with initial crack-like defect.

2. Details of test specimens

The experimental tests are carried out on three CFCST T-joints, two of which are used to fabricate crack by fatigue test and the remaining one specimen is used for comparison. The joint parameters are demonstrated in Table 1. Fig. 1 illustrates the configuration of all the specimens.

All the steel tubes of the specimens are made of Q235B, which is commonly used in structural engineering in China. Before carrying out the static test, the material properties of the steel tubes are measured from tensile coupon test, which are summarized in Table 2. The compressive strength of concrete in the chord is $f_{cu} = 47.6$ MPa, which is obtained from the cubic compressive

test.

In addition, the fracture toughness of steel material is estimated by Charpy V-notch impact test prior to the experimental test. The sub-size specimens are permitted according to the specifications, and the Charpy data are illustrated in Table 3. It can be found that the fracture toughness property of the steel material is considerably qualified.

Table 1 Specimen parameters

Concrete-filled tubular joint parameters	Notation	T-joint
Chord thickness (mm)	T	6
Chord diameter (mm)	D	219
Chord length (mm)	L	1630
Brace thickness (mm)	t	6
Brace diameter (mm)	d	102
Brace length (mm)	l	360
d / D	B	0.47
$D / 2T$	Γ	18.25
t / T	T	1.0

Table 2 Mechanical properties of specimens

	σ_y (MPa)	σ_u (MPa)	E_s (GPa)	Elongation (%)
Chord	288	464	189	36
Brace	325	483	186	30

Table 3 Charpy data

Specimen	Size (mm × mm × mm)	Temperature (°C)	Impact energy (KV ₂) (J)
1			70
2	10 × 5 × 55	20	74
3			63

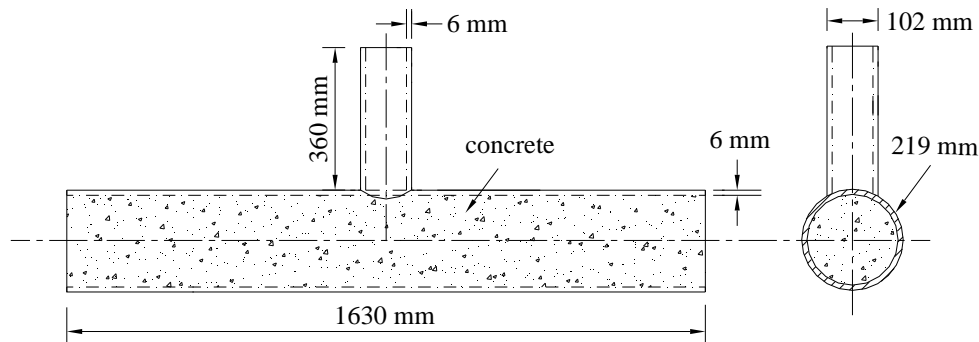


Fig. 1 Dimensions of CFCST T-joint specimen

3. Test scheme

3.1 Test set-up

SDS500 electro-hydraulic servo static/dynamic universal testing machine is used to perform fatigue and static tests, and it is shown in Fig. 2. During the experimental test, the boundary conditions of all the specimens are simulated as a hinge, which is gained by using steel pin to connect the ends of chord and the supports (as shown in Fig. 2). The actuator of the test rig can provide cyclic or axial tensile loadings to the specimens. The actuator can generate axial load with a magnitude of ± 500 kN or axial displacement with a magnitude of ± 75 mm. The displacement at brace end and the applied axial load to the specimens can be collected by data acquisition system automatically in the experimental process.

3.2 Measuring equipment

To obtain the deformation data of the specimens accurately, two LVDTs are used to monitor the displacement of all the specimens, one of which is located at the bottom of chord, and another one is placed at the location of the neutral plane of the chord. Such placement can be found in Fig. 3. The stroke length of the transducers is 100 mm, which is large enough for measuring the displacement in the experimental test because the stiffness of the CFCST joints is remarkably large compared with the tubular joints with hollow section, which ensures that the displacement or the deformation of the CFCST joints is relatively small.

The RMG4015 detector, as shown in Fig. 4, is used to monitor the crack depth under different applied loadings. The range of the measurement is 0~99.9 mm with a precision of 0.1 mm, which is suitable for the common cracked specimens. However, the distance of the crack-depth probe is 2.5 mm, meaning that when the crack mouth opening displacement is larger than 2.5 mm, the crack depth cannot be captured.

The dimensions of the crack mouth opening displacement (CMOD) are measured by using USB microscope camera which can provide high quality images to be convenient for gaining the data of CMOD. Two different magnifications can be taken to adapt to long or adjustable working distance and the precision of the instrument is 0.1 mm. The measuring interface of the camera is presented in Fig. 5.

To estimate the location of the maximum hot spot stress along the weld toe, DH-3816 strain



Fig. 2 View of test rig for CFCST T-joint specimen

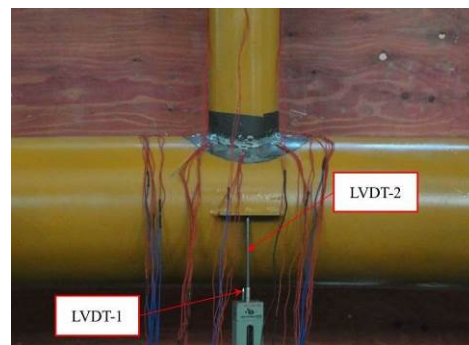


Fig. 3 Placement of LVDTs



Fig. 4 RMG4015 crack depth detector



Fig. 5 Measuring interface of the digital camera



Fig. 6 Placement of strain gauges

acquisition system is used to collect the data of the strain gauges. The strain gauges are placed along the brace/chord intersection at 45° intervals as shown in Fig. 6. At each spot, two strain gauges perpendicular to the weld toe are arranged in a so-called linear extrapolation region specified in CIDECT (2000). The strains perpendicular to the weld toe (ϵ_{\perp}) can be calculated by linearly extrapolating the above two measured strain values directly. At crown and at saddle positions, two strain gauges parallel to the weld toe are also placed to measure the strains in this direction (ϵ_{\parallel}). Similarly, the strains parallel to the weld toe can also be obtained from linear extrapolation method. The stress concentration factor (SCF) at each measuring point perpendicular to the weld toe is calculated from the following equation

$$SCF = \left(\frac{\epsilon_{\perp}}{\epsilon_n} \right) \times \frac{1 + (v\epsilon_{\parallel}/\epsilon_{\perp})}{1 - v^2} \quad (1)$$

Assuming $c = \frac{1 + (v\epsilon_{\parallel}/\epsilon_{\perp})}{1 - v^2}$, Eq. (1) can be expressed as follow

$$SCF = c \times \left(\frac{\epsilon_{\perp}}{\epsilon_n} \right) \quad (2)$$

where v is Poisson's ratio; ϵ_n is the nominal strain.

At each crown and saddle position, the SCF value can be calculated directly from Eq. (2), while for the other measuring points, the value of coefficient c is selected to be the average value of the strains at four measuring points, namely crown and saddle positions.

The hot spot stress at the weld toe can be calculated from the following equation

$$\sigma_{\text{HSS}} = SCF \times \sigma_{\text{nom}} \quad (3)$$

where σ_{nom} is the nominal stress.

4. Experimental investigation

4.1 SCF Measurement

Before carrying out fatigue test, the distribution of hot spot stress along the weld toe of the specimens used for fatigue test (T2 and T3) should be determined to obtain the position of the maximum SCF, which is used to estimate the possible location of fatigue surface crack. The SCF test is conducted under the axial loading applied at the brace end with loading intervals of 12 kN in the range from 0 kN to 60 kN. Additionally, to ensure the accuracy of the calculated SCF value, the values of all the strain gauges under every axial loading are measured for three times, which are collected by the DH-3816 strain acquisition system. The average strain of the three measuring values is used for calculating the SCF from Eq. (1) in Section 3.2. Fig. 7 illustrates the SCF distribution along the weld toe, and it can be clearly found that the maximum value of SCF is located at the crown position, which indicates that the crack will initiate at this location under cyclic loadings. The peak SCF values of the two specimens are quite close since they have identical geometry and are made of same steel and concrete materials. The SCF distribution along the weld toe is not completely symmetrical, and it may be caused by initial imperfection of the specimens or different weld sizes along the intersection.

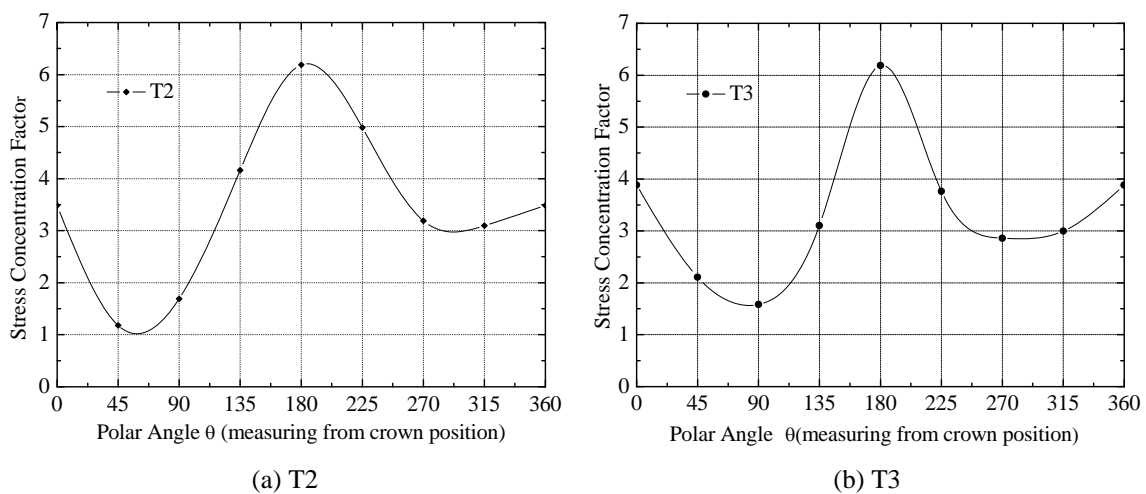


Fig. 7 SCF distribution along weld toe in the specimens

4.2 Fabrication of fatigue crack

Fabrication of crack for the specimens is through fatigue test. According to the experimental results of the SCF distribution, the stress amplitude of fatigue test is determined and it is tabulated in Table 4. The frequency of the applied cyclic loading is 4.0 Hz. The cracks of the two specimens are fabricated after 523,155 and 712,415 cycles respectively. Fig. 8 shows the approximate locations of the fabricated cracks after fatigue test, and it can be seen that the cracks are symmetrically located in the weld toe and they are relatively close to the crown position. The final crack locations are consistent with the measured location of the maximum SCF. The difference occurred between the two specimens (T2 and T3) is the depth of the fabricated crack, being used to study the effect on the static strength of CFCST T-joints. The fatigue test results are summarized in Table 5. From Table 5, it can be found that the depth of cracks is larger than the thickness of the chord wall, especially for specimen T3. The reason why the depth of the crack is larger than the thickness of the chord is that the cracks of the two specimens have both initiated in the weld toe, and then continue to propagate towards the chord wall. Meanwhile, the height of the weld measured by welding angle gauge is 8.0 mm and 6.4 mm, respectively. That is to say, the

Table 4 Stress amplitude of fatigue test

Specimen	T2	T3
Maximum loading (kN)	85.16	78.8
Minimum loading (kN)	7.6	3.5
Axial tension amplitude (kN)	77.56	75.3
Cross section area (mm ²)	1808.64	1808.64
Nominal stress amplitude (MPa)	42.88	41.63
SCF	5.876	6.187
Hot spot stress amplitude (MPa)	252	257.6

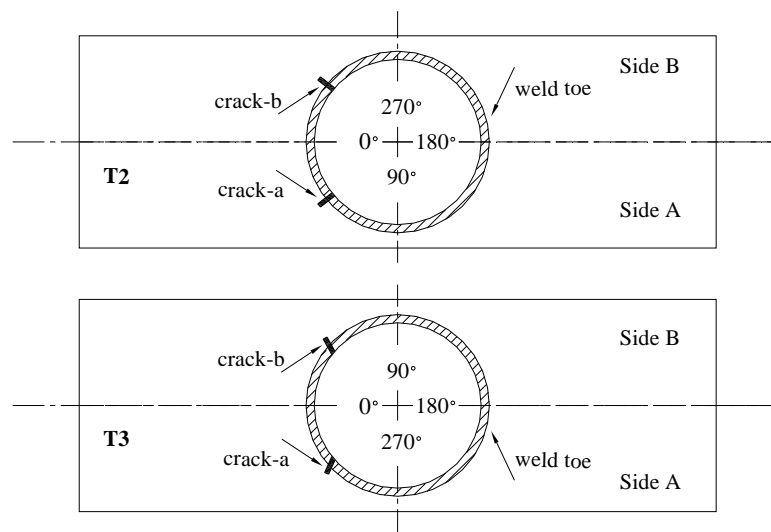


Fig. 8 Position of crack for CFCST T-joints

Table 5 Description of fatigue crack

Specimen	Cracked position (polar angle θ)	Description (crack depth)
T2	About 30° and 330°	Side A 3.9 mm / Side B 6.6 mm
T3	About 45° and 315°	Side A 12.4 mm / Side B 11.2 mm



Fig. 9 Measuring points of cracked specimens

depth of cracks will be less than 14.0 mm for specimen T2, and 12.4 mm for specimen T3, theoretically. After completing the experimental test, the crack surface is not perpendicular to the chord wall from observation, indicating that the depth of the cracks can be a little larger than an estimated thickness based on the sum of the weld toe thickness and the chord wall thickness.

4.3 Static strength test

After fabricating the fatigue crack, the experimental tests on the static strength are carried out for three specimens. For all the specimens, load versus displacement data are obtained by the loading cell of the actuator. In addition, the deformation of the specimens can be gained via the displacement of the chord and the brace, measured by the LVDTs and the loading cell of the actuator respectively. For the specimen T1, the test is stopped when rate of the brace displacement increased rapidly compared with the small increase in loading. Meanwhile, for the cracked specimens T2 and T3, the data of the crack propagation are recorded by the crack depth detector and the USB digital microscope camera at several measuring points, which are shown in Fig. 9. The crack extension curves of the two specimens can then be depicted directly. When the CMOD of the specimens reaches 2.5 mm, which is the distance of the crack-depth probe, the monitor of the crack propagation is ceased. Afterwards, when the load is rarely increased, the static strength test is completed thoroughly.

5. Results and discussion

The experimental results of all specimens are analyzed and summarized in this section. The residual static strength of the cracked specimens can be obtained directly from the load-displacement curves. However, a criterion must be selected to predict the load carrying capacity of the CFSCT T-joints. Much attention should be paid to the fact that the deformation

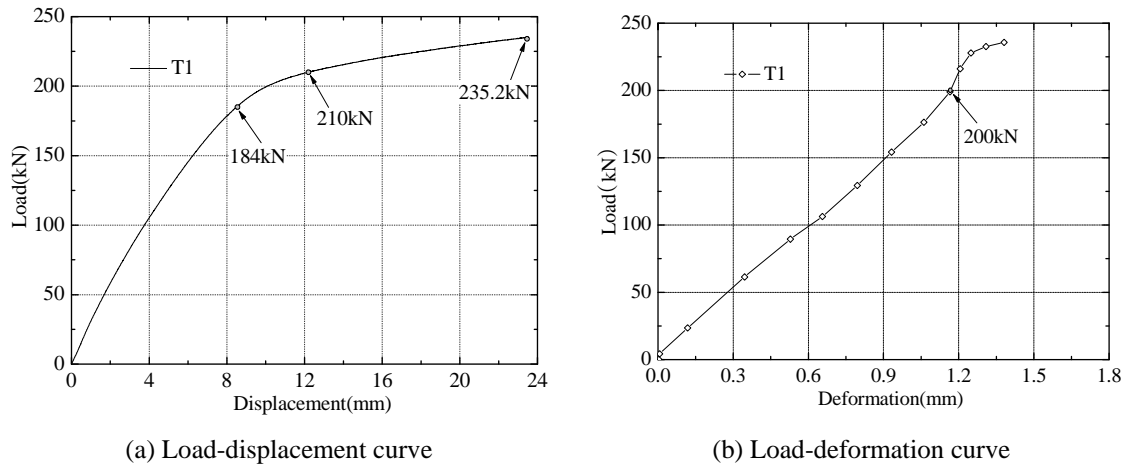


Fig. 10 Experimental curves for T1

limit and the twice-elastic slope criteria, which are used to analyze the ultimate strength of tubular joints with hollow section, cannot be suitable for investigating the CFCST joints due to the subtle deformation of the chord. Therefore, the peak load at the load-displacement curve is considered to be the load bearing capacity for a CFCST joint (Chen and Huang 2009).

5.1 Specimen T1

The load-displacement and the load-deformation curves for specimen T1 are plotted in Fig. 10. The displacement in Fig. 10(a) refers to the displacement at brace end, and the deformation in Fig. 10(b) refers to the difference of the two displacements measured from the LVDTs. As can be seen from the experimental curves, the load of the specimen before reaching yield strength is fully proportional to the displacement, which represents the characteristics of the linear elastic stage. However, the stiffness of the specimen begins to decrease after the load exceeds 184 kN, and the rate of the displacement increases rapidly relative to a small increase in load. The stiffness remains stable when the load exceeds 210 kN. Therefore, it can be regarded as plastic stage of the specimen. According to the definition on the load carrying capacity of CFCST joints, the static strength of the uncracked specimen T1 is considered to be 235.2 kN. For the load-deformation curve, the stiffness in the initial elastic stage implies that the steel and the concrete can work together effectively. When the load is about 200 kN, a small jump occurs in the load-deformation curve. This phenomenon may be caused by the separation of the concrete and the steel tube at the intersection region due to the plasticity accumulation. Afterwards, relatively large deformation occurs mainly on the steel tube under continuous loading. It is noted that the entire deformation of the specimen is 1.38 mm, and such smaller value of deformation verifies the fact that the filled concrete can enhance the stiffness of the joint with hollow section.

The failure mode of specimen T1 is observed directly from the experimental test as shown in Fig. 11. There is no obvious deformation in the region around the intersection, indicating that only relatively small separation between the concrete and the steel tube occurs. No large separation can ensure good cooperation between the two materials and this is advantageous for improving the stiffness. Even at failure state, there is no crack observed along the weld toe in the experimental



Fig. 11 Failure mode for specimen T1

test. However, the chord has a clear flexural deformation after the test, and such deformation cannot restore after unloading. This means large plastic deformation occurs in this specimen during the test. Hence, yielding of the chord under flexure rather than local buckling becomes the dominant failure mode of the uncracked CFCST T-joint.

5.2 Specimen T2

Fig. 12 illustrates the experimental curves of the static strength testing on the cracked specimen T2. The load is linearly related to the displacement up to a load of 151.1 kN. Subsequently, the slope of the load-displacement curve is changed, and in this stage the stiffness of the specimen begins to decrease. The stiffness of the specimen is significantly small after the load reaches a magnitude of 195.9 kN. Such change may be caused by the plastic deformation formed in crack tips during the process of crack propagation. Additionally, it may be due to the crushing of the in-filled concrete around the brace/chord intersection region under the relative large applied loadings. For the load-deformation curve, the stiffness at the initial elastic stage is fully linear. In this stage the crack located at the weld does not propagate rapidly so that the stiffness of the specimen is not deteriorated severely. When the load is up to 177.4 kN, there is a drop in stiffness. The main reason is that the crack has already propagated to a large extent. Meanwhile, a separation occurs between the concrete and the steel tube at the region around the brace/chord intersection.

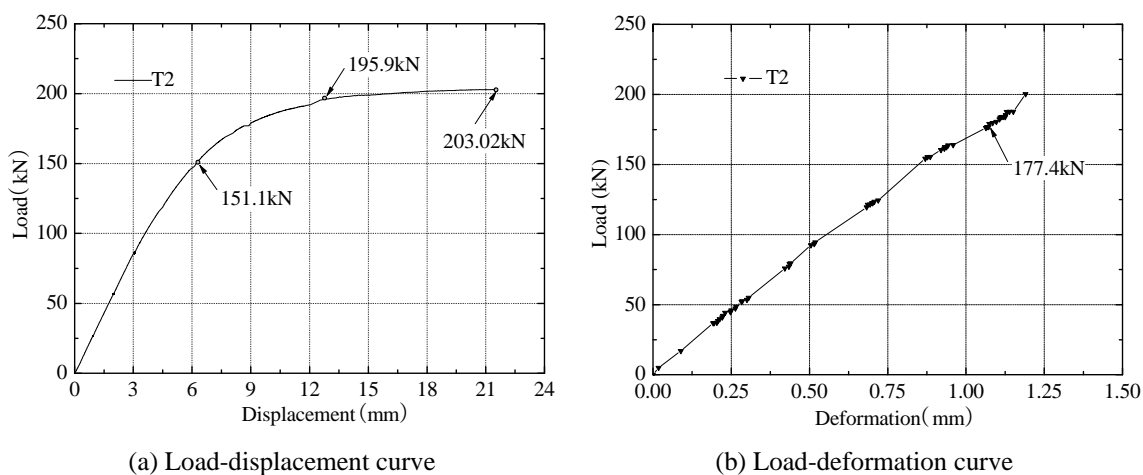


Fig. 12 Experimental curves for T2

The global deformation of the cracked specimen T2 at final stage is 1.19 mm. According to the definition on the load carrying capacity of CFCST T-joints, the static strength of T2 is determined to be 203.02 kN.

Fig. 13 shows the development of the crack depth at various loadings. As the crack occurs almost symmetrically about the crown, one of which, located at a position with a polar angle of 30°, is defined as crack-a, and the other one is denoted as crack-b. From Fig. 13, the depth of crack-a increases with the increasing of the applied axial loading until the load is up to 120 kN. As the crack depth of this specimen is relative small, the fatigue crack can propagate gradually under increasing loadings. However, there is a small increase in crack depth after the applied axial loading exceeds 120 kN. At this loading point, the crack depth in Fig. 13(a) is already larger than 6mm, which value is same to the chord thickness. Since the crack depth has not a clear increase after the load exceeds 120 kN, the crack at this time should penetrate the tube wall, and thus the crack depth cannot increase any more. For crack-b, however, there is a large increase in crack depth before reaching a load of 30 kN. The crack depth is rarely changed with the loading increase after the load exceeds 30 kN, especially for the crack depths at the measuring points within the distance of 20 mm from crack initiation (point 0). Clearly, the crack depth shown in Fig. 13(b) is bigger than 9 mm at some measuring points, and such depth also exceeds the chord thickness. The crack depth does not increase any more at some measuring points because the crack at these points may also penetrate the tube thickness.

Fig. 14 depicts the crack mouth opening displacement (CMOD) for specimen T2. CMOD is remarkably small when the applied load is lower, and it increases gradually with the increasing of the axial loading in initial stage. However, CMOD begins to grow rapidly after the load exceeds a magnitude of 156 kN and 134 kN, particularly 171 kN and 157 kN, for crack-a and crack-b respectively. Such increase of CMOD can be due to the fact that the crack becomes blunt. A blunted crack means large amount of plastic deformation forms around the crack tips. It is also noted that there is no drop of load in CMOD curve, meaning that plastic damage but not brittle fracture occurs.

From experimental test, the failure mode of specimen T2 is shown in Fig. 15. Small deformation

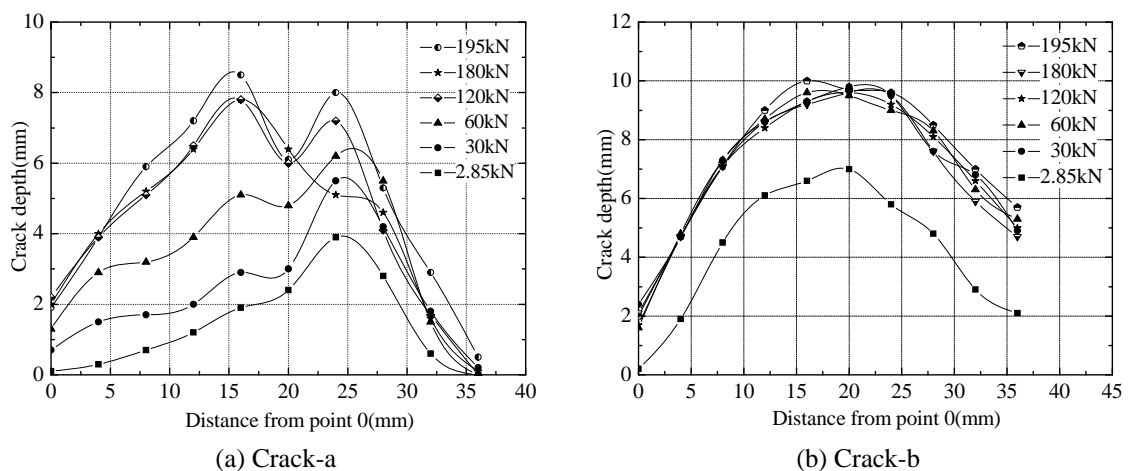


Fig. 13 Crack depth at various loads for T2 (*Note: The point 0 of the curve is the initiation point of crack-a or crack-b)

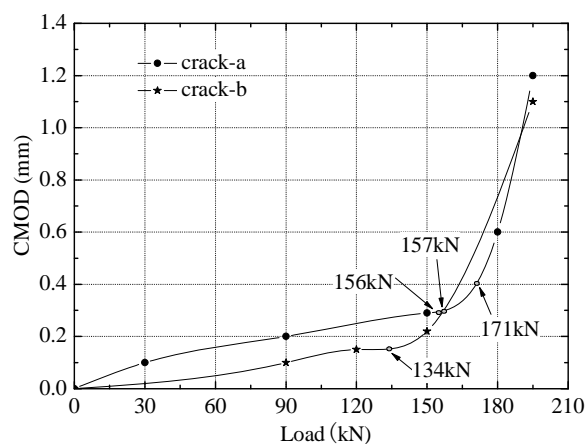


Fig. 14 Crack opening displacement at various loads for T2

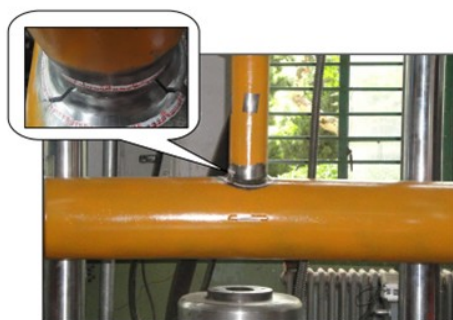


Fig. 15 Failure mode for T2

around the brace/chord intersection can be found directly through observation, which is coincident with the measured deformation value. The much smaller deformation at the intersection represents that the radial stiffness of the chord is improved due to the filled concrete since a large ovalisation of the chord is the dominant deformation for a tubular joint with hollow section. The fatigue crack is located at the weld, and then propagates towards the wall of the chord. Subsequently, the depth and the opening displacement of the crack mouth extend gradually until the joint fails. For the region around the brace/chord intersection, small deformation occurs caused by cracking. Comparatively, the chord has a clear flexural deformation after the test. As such flexural deformation cannot restore after test, plastic failure of the chord under bending becomes a dominant mode for the specimen. Moreover, obvious plastic deformation can be observed at the two ends of the crack because the CMOD at the crack tips cannot recover to its original value after loading is removed. All the plastic deformations of the specimen T2 ensure the cracked joint has a good ductility before fracture.

5.3 Specimen T3

After carrying out the static test on specimen T3, the load-displacement curve and the load-deformation curve are obtained completely, and they are plotted in Fig. 16. The results show

that the stiffness of the specimen is not changed before the value of a load attains to 159 kN. Thereafter, the stiffness decreases gradually as the applied axial load increases. In this stage, the joint enters a yielding state. Once the value of the load exceeds 182.7 kN, the stiffness of the joint is rarely varied any more. After reaching the maximum load with a magnitude of 200.94 kN, the joint is unable to carry loading any more. Hence, the residual static strength of specimen T3 is defined as 200.94 kN.

In the deformation curve, the load is linearly related to the deformation in initial stage. Such linearity indicates that the filled concrete and the steel tube can work together effectively, and no separation between the two materials. The stiffness of the joint declines after the load reaches 175 kN. Such stiffness reduction may be caused by the separation of the concrete and the steel tube at the brace/chord intersection, or may be due to the concrete crushing. In final state, the overall deformation of specimen T3 is only 0.9 mm, and such small value also proves the fact that the radial stiffness of the chord is improved greatly by filled concrete.

The process of crack propagation is recorded under various loadings in the experimental process. As two cracks initiate almost symmetrically about the crown position with polar angles of 45° and 315° respectively, they are also named as crack-a and crack-b respectively. Fig. 17 shows the crack depth development at various loadings. It is clearly found that the crack depth increases gradually with the load increasing, and it is mainly caused by the extension of crack towards to the wall-thickness direction of the brace. For the measuring points within a distance of 30mm from crack initiation (point 0) for crack-a, the crack depths at these points are greatly influenced by the increasing of the axial loading. For crack-b, such distance is about 25 mm. However, the crack depths of all the remaining measuring points along the crack length are scarcely affected by various loadings. Similarly, it should also be focused on the fact that the crack depths at several measuring points on the chord wall are already larger than the thickness of the chord wall. This means the crack at some positions has already penetrated the chord wall, and the crack depth cannot increase any more at these positions.

Fig. 18 illustrates the crack mouth opening displacement (CMOD) for specimen T3. CMOD grows slowly as the applied load increases when the value of the load is less than 136 kN for crack-a and 134 kN for crack-b respectively. However, the CMOD increases suddenly after the

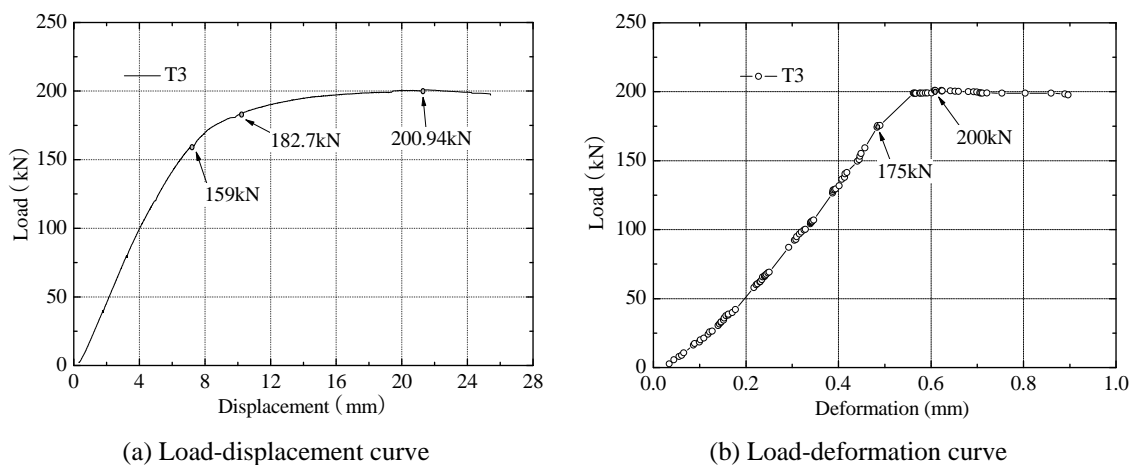


Fig. 16 Experimental curves for specimen T3

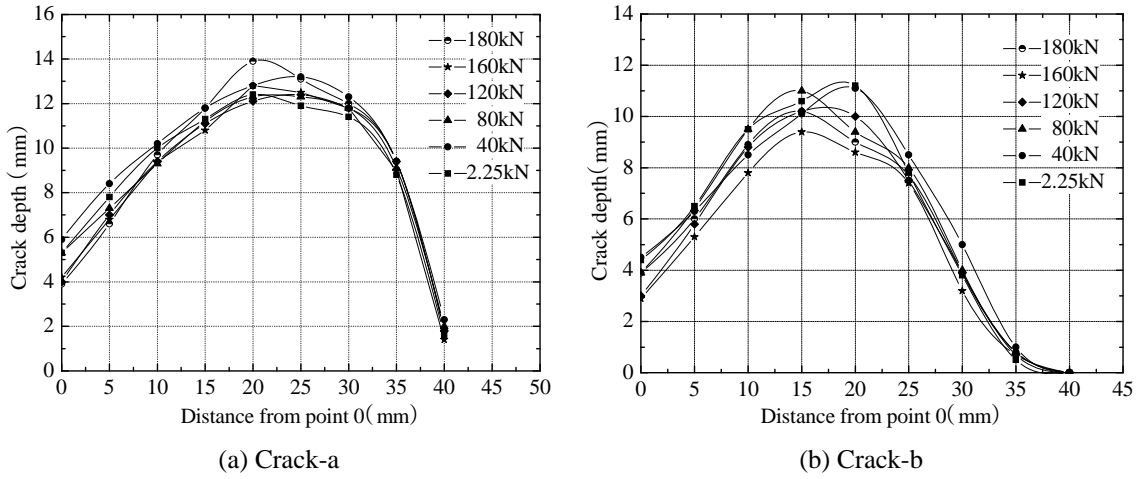


Fig. 17 Crack depth at various loads for T3 (*Note: Point 0 of the curve is the initiation point of crack-a or crack-b)

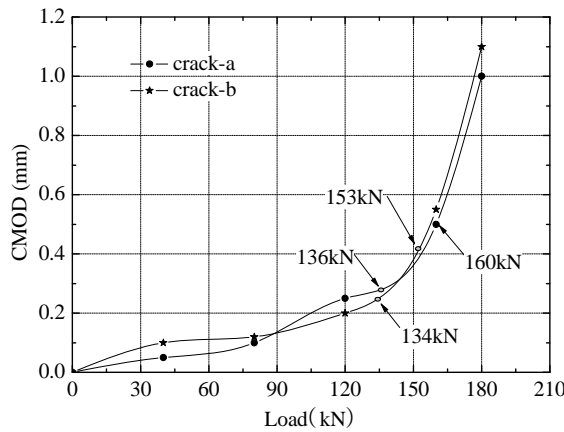


Fig. 18 Crack opening displacement at various loads for T3

load is beyond 160 kN for crack-a and 153 kN for crack-b. This phenomenon demonstrates that a large amount of plastic deformation at the crack tips forms, and the cracks begin to be blunted. No loading drop in the curve proves that this joint fails in the form of plastic strength damage rather than sudden brittle fracture.

Fig. 19 depicts the failure mode of specimen T3. Similarly to the specimen T2, the overall deformation of specimen T3 is also considerably small, and only smaller local deformation can be found at the brace/chord intersection on the chord surface. For specimen T3, the crack hardly propagates in the tube wall-thickness direction because it already penetrates the tube wall at some positions.

Furthermore, plastic deformation is observed both in the chord and at the crack tips. The final failure mode is shown in Fig. 19. The chord still behaves like a flexural beam since local deformation of the chord in radial direction is much smaller compared to the global flexural

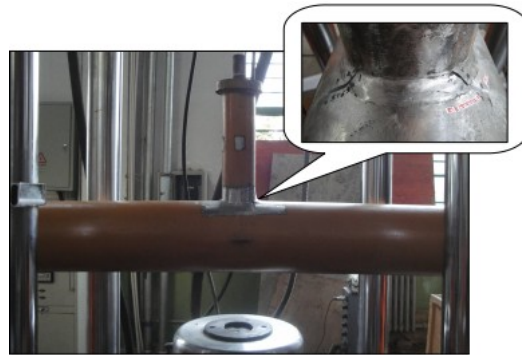


Fig. 19 Failure mode for T3

deformation of the chord. A large plastic flexural deformation still exists after the applied load is removed. Accordingly, CMOD cannot restore to its original value after unloading, which means that there is also plastic deformation at crack tips. In overall, specimen T3 has plastic strength failure rather than brittle fracture failure from experimental observation.

Another interesting phenomenon is noted here that fatigue crack initiates mostly at weld toe on the chord surface for tubular joints with hollow section according to many experimental observations from fatigue tests in the literature. The fatigue crack also propagates along the weld toe on the chord surface, and final failure is plastic strength or fracture failure on the chord.

However, fatigue crack can initiate at the weld based on the experimental results on specimens T2 and T3, and it also propagates through the weld thickness. This means the ductility of the weld should be also considered in the fracture assessment for welded CFCST joints in further study.

5.4 Comparison of experimental results

To study the effect of fatigue crack on the static strength of CFCST T-joints, the load-displacement curves of both cracked and uncracked specimens are analyzed. Fig. 20 illustrates the load-displacement curves of all specimens. It can be seen that the stiffness of the cracked specimens and the uncracked specimen agree very well in initial stage within the load of 160 kN. In this period, the stiffness of the cracked joints is not influenced by the fatigue crack greatly. However, when the axial load exceeds 160 kN, the stiffness of the cracked specimens is different from that of the uncracked specimen. The stiffness of the specimen without crack is larger than that of the specimens with crack. This difference may be possible due to large CMOD and amounts of plastic deformation at crack tips.

From the load-displacement curves, it can be clearly seen that the load carrying capacity of specimens T1 and T2 are 235.2 kN and 203.02 kN respectively. The magnitude of static strength reduction for specimen T2 is up to 13.7%. While for specimen T3, the static strength of the joint is 200.94 kN, which is reduced by 14.6% compared with that of the uncracked specimen T1. In overall, existence of fatigue does not affect the stiffness in linear and elastic stage, but it really deteriorates the static strength. It seems that the fatigue crack does not change the failure mode of CFCST joints although crack may cause steel material to become much brittle around crack front. However, this conclusion is only suitable for Q235B steel because this material has good ductility based on the Charpy test. It is still necessary to conduct further study on investigating the effect of

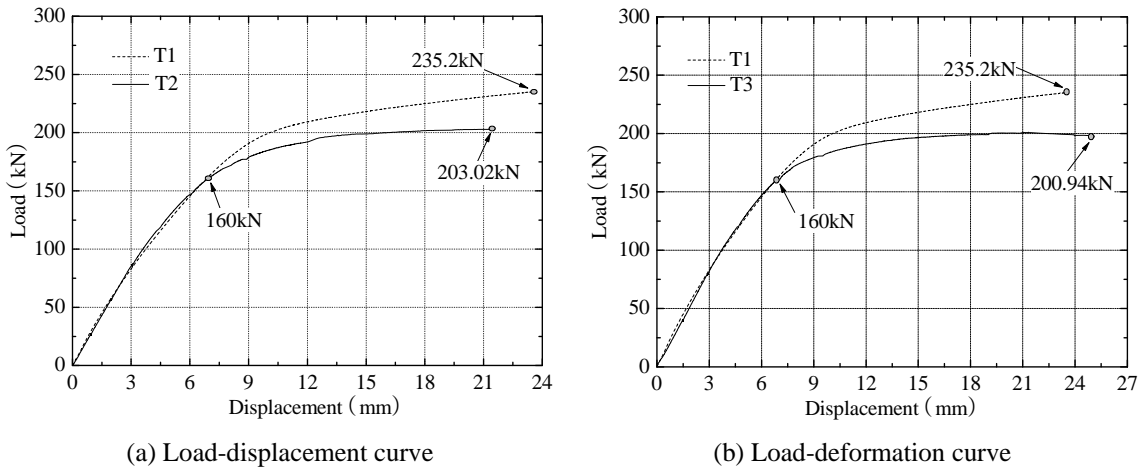


Fig. 20 Load-displacement curves

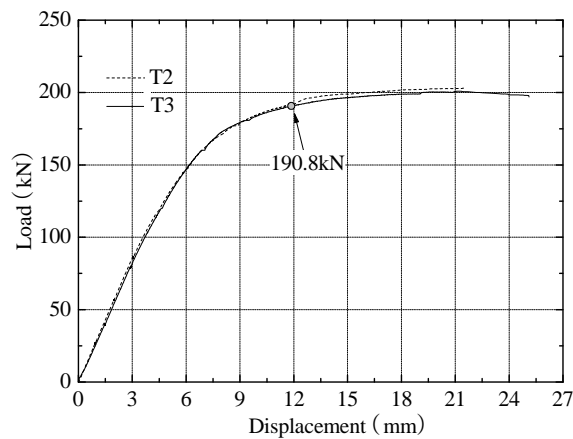


Fig. 21 Comparison of load-displacement curves for cracked specimens

fatigue crack on the failure mode of other steel materials with possible much more brittleness.

5.5 Effect of crack depth on residual static strength

The effect of the crack depth on residual static strength of the cracked specimen is also studied here. For specimen T2, the maximum depth values of crack-a and crack-b are 3.9 mm and 6.6 mm separately. However, such values of crack-a and crack-b for specimen T3 are 12.4 mm and 11.2 mm respectively. Obviously, fatigue crack in specimen T3 has a much bigger depth. Fig. 21 provides the load-displacement curves of specimens T2 and T3 together. It can be seen that the stiffness of the two cracked specimens agrees perfectly with each other before reaching a load of 190.8 kN. The load carrying capacity between specimens T2 and T3 is only 1.02%. Such small difference shows that the effect of the crack depth on residual static strength of cracked CFCST joints is considerably slight.

From the experimental results, it can be found that some benefits may be attributed to the concrete filling, such as the overall displacement and failure mode of the tubular T-joints. In this study, the displacement of the specimens is less than 25 mm when the ultimate carrying capacity is achieved. While, for the hollow tubular T-joints, the displacement of the specimens will be much larger than that of T-joint with concrete filled, which is conducted by Song and Shao (2012). Additionally, Song and Shao (2012) found that larger plastic deformation can occur in the chord as the specimen fails. However, relative small deformation of the chord can be observed in this investigation. Thus, the current test results can be only compared qualitatively with previous study of hollow tubular joints due to the different mechanical property and dimensions of the tubular T-joints used in current and previous study. Moreover, the influence of the cracks on the static strength of hollow tubular T-joints and concrete-filled steel tubular T-joints cannot be compared directly because the size of fatigue cracks occurred between them is also different. Hence, further experimental investigation should be conducted to confirm this point.

6. Conclusions

Static tests of static strength and failure mode on both cracked and uncracked CFCST T-joints are successfully conducted. Through experimental results, the following conclusions can be obtained:

- The stiffness of the cracked specimens is not influenced by the fatigue crack greatly in linear and elastic stage.
- The residual strengths of the cracked CFCST T-joints decrease by 13.7% and 14.6% respectively compared with corresponding uncracked CFCST T-joint. However, the effect of crack depths on the static strength seems to be slight.
- Based on the observation on the failure mode of the two cracked specimens, plastic deformation of the chord under flexure and plastic deformation accumulation at crack tips ensure the CFCST joints have plastic strength failure rather than brittle fracture failure at crack tips. The CFCST joints still have good ductility even fatigue crack initiates at weld.

However, the above conclusions are generalized based on only two specimens. Further experimental tests are strongly recommended to investigate if such conclusions are still effective for CFCST joints with other geometries. In addition, the presented experimental tests are based on Q235B steel materials, it is still uncertain if these conclusions are similar for other steel materials

References

- Burdekin, F.M. (2002), "The fracture behaviour of welded tubular joint-an ESIS TC1-3 round robin on failure assessment methods Part III-UK BS7910 methodology", *Eng. Fract Mech.*, **69**(10), 1119-1127.
- Chen, B.C. and Huang, W.J. (2009), "Experimental study on ultimate bearing capacity of CFST directly-welded K-joints", *China Ci*, **42**(12), 91-98.
- Chiew, S.P., Lie, S.T., Lee, C.K. and Huang, Z.W. (2004), "Fatigue performance of cracked tubular T joints under combined loads. I: Experimental", *Struct. Eng.*, **130**(4), 562-571.
- Chiew, S.P., Lee, C.K., Lie, S.T. and Ji, H.L. (2007), "Fatigue behaviors of square-to-square hollow section T-joint with corner crack. I: Experimental studies", *Eng. Fract Mech.*, **74**(5), 703-720.
- Chiew, S.P., Lee, C.K., Lie, S.T. and Nguyen, T.B.N. (2009), "Fatigue study of partially overlapped circular hollow section K-joints Part 2: Experimental study and validation of numerical models", *Eng. Fract.*

- Mech.*, **76**(15), 2408-2428.
- CIDECT (2000), *Design Guide for Circular and Rectangular Hollow Section Joints under Fatigue Loading*, Germany.
- Lee, C.K., Chiew, S.P., Lie, S.T. and Ji, H.L. (2007), "Fatigue behaviors of square-to-square hollow section T-joint with corner crack. II: Numerical modeling", *Eng. Fract. Mech.*, **74**(5), 721-738.
- Lee, C.K., Chiew, S.P., Lie, S.T. and Nguyen, T.B.N. (2009), "Fatigue study of partially overlapped circular hollow section K-joints Part 1: Geometrical models and mesh generation", *Eng. Fract. Mech.*, **76**(16), 2445-2463.
- Lie, S.T., Yang and Z.M. (2009), "Fracture assessment of damaged square hollow section (SHS) K-joint using BS7910:2005", *Eng. Fract. Mech.*, **76**(9), 1303-1319.
- Lie, S.T., Chiew, S.P., Lee, C.K. and Huang, Z.W. (2004), "Fatigue performance of cracked tubular T joints under combined loads. II: Numerical", *Struct. Eng.*, **130**(4), 572-581.
- Lie, S.T., Chiew, S.P., Lee, C.K. and Yang, Z.M. (2006a), "Static strength of cracked square hollow section T joints under axial loads. I: Experimental", *Struct. Eng.*, **132**(3), 368-377.
- Lie, S.T., Lee, C.K., Chiew, S.P. and Yang, Z.M. (2006b), "Static strength of cracked square hollow section T joints under axial loads. II: Numerical", *Struct. Eng.*, **132**(3), 378-386.
- Lie, S.T., Zhang, B.F. and Shao, Y.B. (2007), "Residual strength of cracked circular hollow section (CHS) tubular K-joints", *Proceedings of the 9th International Conference on Steel, Space & Composite Structures*, Yantai & Beijing, China, October.
- Lie, S.T., Yang, Z.M. and Gho, W.M. (2009), "Validation of BS7910:2005 failure assessment diagrams for cracked square hollow section T-, Y- and K-joints", *Int. J. Pres. Ves. Pip.*, **86**(5), 335-344.
- Marshall, G.W. and Ainsworth, R.A. (2002), "The fracture behaviour of welded tubular joint-an ESIS TC1-3 round robin on failure assessment methods Part II: R6 analysis", *Eng. Fract. Mech.*, **69**(10), 1111-1118.
- Schindler, H.J., Primas, R. and Veidt, M. (2002), "The fracture behaviour of a welded tubular joint: An ESIS round robin on failure assessment methods Part V: Screening method by required toughness and plastic stability considerations", *Eng. Fract. Mech.*, **69**(10), 1149-1160.
- Song, S.Z. and Shao, Y.B. (2012), "Study on static strength of circular tubular T-joints with fatigue crack", *Steel Constr.*, **S**, 509-517. [In Chinese]
- Talei-Faz, B., Brennan, F.P. and Dover, W.D. (2004), "Residual static strength of high strength steel cracked tubular joints", *Mar. Struct.*, **17**(3-4), 291-309.
- Yang, Y.X. (1992), "The research of performance of tubular T-joints with fatigue crack", *J. Zhengzhou Inst. Technol.*, **13**(1), 42-46.
- Yang, Z.M., Lie, S.T. and Gho, W.M. (2007), "Failure assessment of cracked square hollow section T-joints", *Int. J. Pres. Ves. Pip.*, **84**(4), 244-255.
- Zerbst, U. and Miyata, T. (2002), "The fracture behaviour of a welded tubular joint-an ESIS TC1.3 round robin on failure assessment methods Part VI: Application of WES 2805-1997", *Eng. Fract. Mech.*, **69**(10), 1161-1169.
- Zerbst, U., Heerens, J. and Schwalbe, K.H. (2002a), "The fracture behaviour of welded tubular joint-an ESIS TC1.3 round robin on failure assessment methods Part I: Experimental data base and brief summary of the results", *Eng. Fract. Mech.*, **69**(10), 1093-1110.
- Zerbst, U., Primas, R., Schindler, H.J., Heerens, J. and Schwalbe, K.H. (2002b), "The fracture behaviour of a welded tubular joint-an ESIS TC1-3 round robin on failure assessment methods Part IV: Application of the ETM 97/1", *Eng. Fract. Mech.*, **69**(10), 1129-1148.